Modifiers of prion protein biogenesis and recycling identified by a highly-parallel endocytosis kinetics assay

Ballmer, Boris A ; Moos, Rita ; Liberali, Prisca ; Pelkmans, Lucas ; Hornemann, Simone ; Aguzzi, Adriano

Abstract: The cellular prion protein, PrPC, is attached by a glycosylphosphatidylinositol anchor to the outer leaflet of the plasma membrane. Its misfolded isoform PrPSc is the causative agent of prion diseases. Conversion of PrPC into PrPSc is thought to take place at the cell surface or in endo-lysosomal organelles. Understanding the intracellular trafficking of PrPC may therefore help elucidating the conversion process. Here we describe a time-resolved fluorescence resonance energy transfer (FRET) assay reporting membrane expression and real-time internalization rates of PrPC The assay is suitable for high-throughput genetic and pharmaceutical screens for modulators of PrPC trafficking. Simultaneous administration of FRET donor and acceptor anti-PrPC antibodies to living cells yielded a measure of PrPC surface density, whereas sequential addition of each antibody visualized the internalization rate of PrPC (Z'-factor > 0.5). RNA interference assays showed that suppression of AP2M1, RAB5A, VPS35 and M6PR blocked PrPC internalization, whereas downregulation of GIT2 and VPS28 increased it. PrPC cell surface expression was reduced by downregulation of RAB5A, VPS28 and VPS35, and enhanced by silencing EHD1. These data identify a network of proteins implicated in PrPC trafficking, and demonstrates the power of this assay for identifying modulators of PrPC trafficking.

DOI: https://doi.org/10.1074/jbc.M116.773283

JBC Papers in Press. Published on March 24, 2017 as Manuscript M116.773283
The latest version is at http://www.jbc.org/cgi/doi/10.1074/jbc.M116.773283

Modifiers of prion protein biogenesis and recycling identified by a highly-parallel endocytosis kinetics assay

Boris A. Ballmer[1], Rita Moos[1], Prisca Liberali[2,3], Lucas Pelkmans[3], Simone Hornemann[1], Adriano Aguzzi[1]

From the Institute of Neuropathology, University of Zurich, Zurich, Switzerland[1], Institute of Molecular Life Sciences, University of Zurich, Zurich, Switzerland[2], Friedrich Miescher Institute for Biomedical Research, Basel, Switzerland[3]

Running title: *TR-FRET assay to detect PrP^C membrane expression and internalization rates*

To whom correspondence should be addressed: Dr. S. Hornemann and Prof. A. Aguzzi, University of Zurich, Institute of Neuropathology, Schmelzbergstrasse 12, CH-8091 Zurich, Switzerland, Telephone: (41) 44 255 21 07; FAX: (41) 44 255 44 02; E-mail:simone.hornemann@usz.ch and E-mail:adriano.aguzzi@usz.ch

Keywords: prion diseases, cell surface, endocytosis, FRET, high-throughput

ABSTRACT

The cellular prion protein, PrP^C, is attached by a glycosylphosphatidylinositol anchor to the outer leaflet of the plasma membrane. Its misfolded isoform, PrP^{Sc}, is the causative agent of prion diseases. Conversion of PrP^C into PrP^{Sc} is thought to take place at the cell surface or in endo-lysosomal organelles. Understanding the intracellular trafficking of PrP^C may therefore help elucidating the conversion process. Here we describe a time-resolved fluorescence resonance energy transfer (FRET) assay reporting membrane expression and real-time internalization rates of PrP^C. The assay is suitable for high-throughput genetic and pharmaceutical screens for modulators of PrP^C trafficking. Simultaneous administration of FRET donor and acceptor anti-PrP^C antibodies to living cells yielded a measure of PrP^C surface density, whereas sequential addition of each antibody visualized the internalization rate of PrP^C (Z'-factor > 0.5). RNA interference assays showed that suppression of AP2M1, RAB5A, VPS35 and M6PR blocked PrP^C internalization, whereas downregulation of GIT2 and VPS28 increased it. PrP^C cell surface expression was reduced by downregulation of RAB5A, VPS28 and VPS35, and enhanced by silencing EHD1. These data identify a network of proteins implicated in PrP^C trafficking, and demonstrates the power of this assay for identifying modulators of PrP^C trafficking.

The infectious agent causing prion diseases (1) is a misfolded and aggregated isoform (PrP^{Sc}) of the host-encoded cellular prion protein (PrP^C). The primary translation product of PrP^C is cotranslationally translocated to the rough endoplasmic reticulum (2), where it undergoes the addition of N-linked oligosaccharide chains, the formation of an intramolecular disulfide bond, and the attachment of a glycosylphosphatidylinositol (GPI) anchor (3). Distal sorting delivers PrP^C to the plasma membrane where it resides in lipid rafts (4). Mature PrP^C is then recycled between the plasma membrane and the endocytic compartment (5).

Several processes have been reported to participate in the endocytosis of PrP^C (6–8). PrP^C located in lipid rafts may be internalized by caveolin/dynamin-dependent endocytosis. PrP^C is transported via caveosomes to early endosomes or to lysosomes for degradation. Alternatively, internalization of PrP^C may be mediated by a clathrin-dependent process (9–11) whereby PrP^C migrates to clathrin-coated pits and is then transported to early endosomes. Dynamin-independent endocytosis pathways may also be involved. This process may be crucial for the conversion of normal PrP^C into PrP^{Sc}, as the conformational change seems to take place at the cell surface and/or in the endocytic pathway. Real-time measurements of PrP^C internalization are therefore

of high interest and might eventually help identifying therapeutic targets against prion diseases.

Fluorescence resonance energy transfer (FRET)-based methods are widely used for the detection of proteins (12) and to validate the proximity of proteins in cells and tissues (13). FRET is a quantum-mechanical process that transmits energy from an excited donor molecule to an acceptor molecule, resulting in red-shifted fluorescence emission by the latter (14). Time-resolved FRET methods based on the use of Europium and allophycocyanin (APC) as donor and acceptor, respectively, allows for homogeneous-phase assays in the absence of background fluorescence (15). The long fluorescence lifetime of Europium leads to a high signal-to-noise ratio and is thus suited to high-throughput applications.

In the present study, we applied the FRET technology to the development of a robust and sensitive quantification assay for PrP^C internalization. The assay was designed to detect either cell surface expression of human PrP^C or the internalization rate of PrP^C in living cells. For the detection of PrP^C on the cell surface, anti-PrP antibodies were added simultaneously, whereas the addition of the two FRET components at different time points enabled the measurement of the endocytosis rate of surface-resident PrP^C by signal subtraction. Furthermore, we show that this assay can be used to identify drugs and genes that modulate PrP^C surface expression and PrP^C endocytosis.

RESULTS

A homogeneous-phase TR-FRET immunoassay for PrP — We first developed a homogeneous TR-FRET immunoassay for the detection of recombinant mouse PrP (residues 23-231; recPrP) and PrP^C in cell lysates. The principle of the assay is shown in Figure 1. We tested several candidate antibodies from an in-house PrP-targeted antibody collection designated as POM antibodies (16), and the previously characterized 3F4 antibody (17), for their efficiency in this type of assay. Some of these antibodies target linear epitopes in the N-terminal, unstructured "flexible tail" of PrP, whereas others recognize discontinuous, conformational epitopes within the C-terminal globular domain of PrP (18–20). Antibodies were coupled to the Europium chelate (Eu) donor or the allophycocyanin (APC) acceptor fluorophores. Various permutations of antibodies in both donor and acceptor functions were tested for their capability to detect recombinant and normal PrP^C in-solution. We predicted, and confirmed experimentally, that repetitive binding of the POM2 antibody to the multiple octapeptide repeats of PrP would allow for simultaneously utilization as both donor and acceptor antibody (Figure 1).

Among the different antibody FRET pairs, the antibody combination POM1-Eu/POM2-APC exhibited a satisfactory dynamic range over 3 logs (125 pg/ml – 100 ng/ml) for the detection of recPrP diluted in crude Hpl $PrnP^{-/-}$ cell lysate, an immortalized hippocampal cell derived from $Prnp^{-/-}$ mice (21), (Figure 2A) with signal linearity between 0.125 and 8 ng/ml (Figure 2B). A lower detection limit (LDL) of < 0.125 ng/ml was determined for the detection of recPrP.

We next assessed the specificity of the assay for PrP^C. We prepared serial dilutions of murine N2a PK1 cell lysates in Hpl $PrnP^{-/-}$ cell lysates, followed by FRET measurement using POM1-Eu/POM2-APC for the detection of PrP^C. PrP^C was detected in lysates across a wide dynamic range (16-500 µg/ml) (Figure 2C) with excellent linearity (Figure 2D). A lower detection limit (LDL) of < 20 µg/ml of crude cell extract was determined for the detection of PrP^C in cells.

The performance of the TR-FRET-based immunoassay was further characterized by various validation parameters and their defined acceptance criteria: the coefficient of variance (%CV), the signal-to-noise ratio (S/N), and the Z' factor (22), a widely used indicator for high-throughput suitability. A Z' factor greater than 0.5 is generally considered sufficient for cell-based high-throughput campaigns. These data are listed in Table 1.

Hence, the above data demonstrate a robust and accurate performance of the assay with high specificity, which makes it suitable for the detection of both recPrP and PrP^C in high-throughput assays.

Design and development of cell surface PrP FRET immunoassays — PrP^C is present at the surface of neurons and on various non-neuronal tissues and leukocytes (23). To adapt our assay to human cells, we first assessed PrP^C expression in several cell lines using a PrP^C-specific ELISA (Figure S1). The human lung epithelial cell line A549 and HeLa cells

were identified as human cell lines with the highest total PrP^C expression. To identify the most efficacious antibody pair enabling detection of PrP^C by FRET, several POM antibodies were again screened in various combinations of FRET donors and acceptors for A549 cells (Figure S2). The FRET pair POM2-Eu/POM2-APC, which binds to the octapeptide repeats (Figure 1), yielded the highest FRET signals within the POM antibody library. As this antibody pair also yielded a good signal for HeLa cells (Figure S2), we selected it for further use in the assay.

We then determined the optimal cell number to be used in the assay by plating different numbers of HeLa and A549 cells, respectively, into 384-well plates. On the following day, cells were washed with ice-cold Tris-Krebs buffer and labeled with POM2-Eu/POM2-APC for 30 min at 4°C. A cell number-dependent FRET signal was detected in a large dynamic range for both human cell lines without washing (homogeneous time-resolved FRET (HTRF) mode) which is more suited for automated HTS applications and after washing out unbound antibodies (TR-FRET mode) (Figure 3A), whereas no signal was obtained for PrP-deficient cells (Hpl $PrnP^{-/-}$) used as negative control. These results confirmed the specificity of the assay.

For A549 cells, a linear dynamic range was found between 500-4000 cells/well (R^2 = 0.69) (Figure 3B and C) in HTRF mode. The linear correlation was improved (R^2 = 0.94) in TR-FRET mode (Figure 3D and E). Similar results were obtained when titrating numbers of HeLa cells using the same antibody pair (Figure 3F and H). Again, essentially linear dynamic ranges were found from 500 to 8000 cells/well in the HTRF mode (R^2 = 0.90) and in the TR-FRET mode (R^2 = 0.98) (Figure 3G and I). For both cell lines and in both measurement modes, 500 cells were sufficient to generate a statistically reliable FRET signal. Assay performance acceptance criteria of Z' factors >0.5, CV values <10% and S/N values >8 were achieved for HeLa cells in the range of 8K to 32K cells in TR-FRET and HTRF mode and for A549 in the range of 2K to 32K cells in the TR-FRET and 32K cells in the HTRF mode (Table 2).

These data validated the assay as a robust and accurate assay for the detection of cell surface PrP^C on intact cells under these conditions.

Manipulation of human PrP cell surface expression on living cells using HTRF and TR-FRET — We then assessed the applicability of the assay to the detection of cell-surface PrP^C. 500 intact, viable cells were preincubated with varying concentrations of unlabeled POM2 antibody. After removing unbound POM2 by washing, cells were incubated with labeled POM2-Eu/POM2-APC. Results in the HTRF (Figure 4A) and TR-FRET mode (Figure 4B) showed an increase in the FRET signal intensity with decreasing concentrations of unlabeled POM2 antibody, as expected from binding site saturation by competing antibodies.

To control the level of PrP^C cell surface expression on intact cells, the GPI anchor of PrP^C was enzymatically cleaved with phosphatidylinositol-specific phospholipase C (PI-PLC). A549 cells were initially labeled with POM2-Eu/POM2-APC and exposed to different concentrations of PI-PLC. FRET signals of cell-surface retained and released PrP^C were measured after transferring the supernatant into a new plate (Figure 4C and D). With increasing PI-PLC concentrations, we found decreasing levels of surface PrP^C and elevated levels of PrP^C in the supernatant. To monitor cytotoxicity of PI-PLC exposure on A549 cells, we established an alamarBlue® cell viability assay (Figure S3). No effect of PI-PLC treatment on A549 cell viability was detectable (Figure S3).

We next tested the performance of the assay in detecting the pharmacological manipulation of PrP^C surface expression in living HeLa and A549 cells. Cells were treated with 0-10 µg/ml brefeldin A (BFA) diluted in 0.75% DMSO (24). BFA inhibits the transport of proteins from the ER to the Golgi apparatus, and thus reduces their display at the cell surface. We found that a BFA concentration of 1 µg/ml in 0.75% DMSO decreased the PrP^C expression level at the cell surface of about 66% in the HTRF (Figure 4E) and about 75% in the TR-FRET mode (Figure 4F) without affecting the cell viability.

Next, we investigated the applicability of our assay to the genetic manipulation of the cell surface PrP^C expression of intact A549 cells. We first used a siRNA targeting the human PRNP gene. The PRNP siRNA was also fully functional as shown by qPCR (Figure S5) and had no toxic effects on the cells as monitored by the alamarBlue assay (Figure S4). We found

that the siRNA efficiently downregulated the expression of PrP^C on the surface of living A549 cells in a concentration-dependent manner ($p < 0.0001$), whereas scrambled siRNAs used as negative controls had no significant effect on PrP^C expression (Figure 4G). Complete suppression was reached at a concentration of 50-100 nM siRNA, as shown by a comparison of the Net-FRET signal to those of Hpl PrnP$^{-/-}$ deficient cells.

These data demonstrate that the assay can be applied to high-throughput pharmacological and genetic PrP^C cell surface manipulation screens.

PrP endocytosis measured by FRET — In a next step, we modified the assay format towards a PrP^C endocytosis assay to assess its suitability for the identification of modifiers controlling the cell surface expression and endocytosis of PrP^C. The principle of the modified assay is shown in Figure 5A. In a first set of experiments, various antibody combinations and cell culture conditions were tested. Satisfactory results were obtained with A549 cells cultured in DMEM medium (without phenol red, antibiotics and FBS) during endocytosis using the antibody combination POM2-Eu/POM2-APC. After labeling A549 cells with POM2-Eu, free antibodies were removed by washing and endocytosis was induced at 37°C after 5 minutes pre-incubation. At specified time points (t = 0-70 min) POM2-APC was added to different wells (15 time points à 6 wells). After the last addition of POM2-APC at 70 min, FRET signals were measured for all wells (Figure 5B). A gradual decrease of Eu-POM2-labeled cell surface PrP^C was observed over time; the decrease was almost linear between 0-30 min ($R^2 = 0.79$; Figure 5C). Similar data were also obtained for HeLa cells (Figure S6A). We found that PrP^C undergoes endocytosis also when antibodies are added in a reversed order (Figure S6B). The endocytosis rate of PrP^C was calculated according to the uptake formula (see Experimental Procedure). After 30 minutes of incubation, 80% of cell surface-resident PrP^C was endocytosed (Figure 5D) which is in agreement with previously reported half-times for PrP^C internalization (5).

Pharmacological blocking of PrP endocytosis pathways — We then used the endocytosis assay to gauge the effects of compounds inhibiting clathrin-mediated endocytosis (chlorpromazine/CPZ) and clathrin-independent uptake (methyl-beta-cyclodextrin/MbetaCD) on internalization of PrP^C in A549 cells (25). CPZ causes clathrin lattices to assemble on endosomal membranes and prevents the assembly of coated pits at the plasma membrane (26), whereas MbetaCD selectively extracts cholesterol from the plasma membrane (27). Cells were pre-treated for 30 min with CPZ or MbetaCD in a dose-dependent manner and subsequently labeled with POM2-Eu (Figure 6). After 30 min of incubation at 37°C, POM2-APC was added and inhibition of PrP^C uptake was assayed by TR-FRET. Figure 6A represents the internalization of PrP^C in A549 cells in the presence of CPZ. CPZ decreased the entry of PrP^C in A549 cells in a dose-dependent manner. A concentration of 0.28 µM CPZ was sufficient to block clathrin-mediated endocytosis of PrP^C without affecting the cell viability of A549 cells as determined in an alamarBlue assay (Figure 6B). On the other hand, a concentration of 5 mM MbetaCD inhibited the uptake of PrP^C without any toxic effect on cell viability as monitored by an alamarBlue assay (Figure 6C and D). The combination of CPZ and any inhibitor blocking clathrin-mediated internalization did not cause any further decrease in the uptake of PrP^C. These data support recent findings on MbetaCD in initiating PrP^C endocytosis (28) and the importance of cholesterol for the endocytosis of PrP^C (29) as well as the inhibitory effect of CPZ on the internalization of PrP^C (30).

Identification of genes that differently impact cell surface expression and endocytosis of PrP — Next, the potential of the endocytosis assay towards genetic manipulations was tested by using seven hand-picked small interfering RNAs (siRNA) targeting major proteins of the membrane-trafficking machinery and their downstream organelles (Figure 7 and Table 3). We expected that some of these siRNAs would modify the endocytosis rate and cell-surface expression of PrP^C, resulting in a reduced FRET signal. The efficacy of PRNP knock-down was again controlled using a siRNA targeting the PRNP gene, whereas untreated cells acted as a negative control. The functionality of the siRNAs was verified by quantitative PCR (Figure S5) and potential toxic effects of the siRNAs to the cells were controlled by performing cell viability assays (Fig-

ure S4).

We found that the knockdown of the small GTPase protein Rab5a, which controls clathrin-dependent endocytosis (31–33) and early endosome dynamics (34), significantly reduced the cell surface expression (t0) and strongly blocked the endocytosis (t0-t30) of PrP^C (Figure 7 and Table 4). Also AP2M1 (AP-2 adaptor protein), a gene involved in clathrin-dependent endocytosis pathways (35) blocked the uptake of PrP^C. Other genes, such as M6PR (Mannose-6-phosphate receptor) (36) and VPS35 (vacuolar protein sorting 35 homolog) (37), which are involved in retrograde transport of proteins from endosomes to the trans-Golgi network, also suppressed the internalization of PrP^C. Moreover, the VPS35 protein was recently shown to reduce the expression of alpha-synuclein in a prion-like seeding model in transgenic mice, thus protecting them from neurodegeneration (38). We also tested EHD1, a gene that encodes the EH domain-containing protein 1 that is involved in endocytosis (39). Suppression of EHD1 slightly increased the cell surface expression level (t0) of PrP^C (Figure 7 and Table 4 without affecting endocytosis. For VPS28, a gene that encodes the vacuolar protein sorting-associated protein 28 homologue involved in endosomal sorting of cell surface receptors (40), an increased endocytosis rate and reduced PrP^C cell surface expression was found. Silencing of GIT2, a gene that encodes the ARF GTPase-activating protein GIT2 (41) increased the uptake of PrP^C without affecting PrP cell surface level (Figure 7). Hence, we were able to identify a number of genes involved in clathrin-dependent internalization of PrP^C and its trafficking to early endosomes. This demonstrates the potential of the assay for comprehensive high-throughput screens of compounds and genes that target the internalization and endocytosis pathway of PrP^C.

DISCUSSION

The exposure of PrP^C at the surface of target cells is a precondition to prion replication and to prion neurotoxicity (42, 43). Several studies have shown that masking PrP^C with antibodies (44) or suppressing its expression with siRNA (45) can reduce prion replication and prolong the life of prion-infected mice. Therefore, an in-depth understanding of the factors controlling PrP^C expression at the cell surface may pave the way to treating human prion diseases.

High-throughput screening platforms to identify modulators of the transcription, translation and protein cycling turnovers that regulate cellular PrP may point to druggable targets, which could be used to selectively reduce human PrP^C in the treatment of CJD patients (46). Being a single-pot method, FRET is suitable to high-throughput assay formats. However, FRET does not allow for the extensive signal amplification afforded by enzyme-linked immunoassays. We therefore wondered whether FRET-based PrP^C detection in high-density microtiter plates would provide the analytical power necessary for this type of assay. Indeed, the assays described here provide high scalability, high specificity, a wide dynamic range and sensitive detection that compares well with enzyme-linked immunosorbent assays (47). Moreover, the assays exhibit broad dynamic ranges and were found to be highly target-specific by spiking, competition and blocking experiments, and required only nanomolar quantities of antibodies. The large detection window and the Z' factor finally allowed us to identify compounds and genes that differently impact the cell surface expression and endocytosis rate of normal PrP^C, thus demonstrating the practicality of the FRET assays for HTS applications in a 384-well format (46, 48).

We then studied the applicability of the FRET-based immunoassays for the simultaneously identification of compounds and genes that differently affect the level and internalization rate of cell surface PrP^C. We first studied the internalization of endogenously expressed human PrP^C on cells. A cell surface half life time of about 25 min of PrP^C was determined – which is in agreement with previous results (5). No PrP^C was detectable in the culture medium during the endocytosis experiment, confirming that PrP^C is mainly endocytosed rather than released from the cell surface. We also observed no loss of FRET signal intensity over the whole time period (75 min) of the cell-surface PrP^C FRET assay, indicating that the PrP-mAbs-Eu complex is stable in our experimental settings. We further conclude from the good agreement of our internalization rate with previously published results (5) that the stability of the PrP-mAbs-Eu complex is also not significantly affected in endosomal compartments and that the binding

of POM2, even if it might modulate interactions of PrP^C with other membrane proteins had no significant effect on PrP endocytosis. In control experiments, MbetaCD and CPZ inhibited endocytosis of PrP^C without affecting cell viability at the chosen concentrations as already reported earlier (31, 49).

We tested the suitability of the FRET-based endocytosis assay for the identification of cell surface and endocytosis modulators of PrP^C. The siRNAs repressing RAB5A and AP2M1 (encoding the μ subunit of the AP-2 complex) showed the strongest inhibition of PrP^C internalization. These data suggest clathrin-mediated endocytosis of PrP^C, as hypothesized by earlier studies showing that AP-2 co-localizes with PrP^C (10). Rab5a suppression brought about a strong reduction in PrP^C cell surface expression and completely blocked the endocytosis of PrP^C after 30 minutes. Similar results were reported by Magalhaes et al. (46), who showed that green fluorescent protein (GFP)-tagged PrP^C, but not GFP-GPI, is endocytosed via Rab5-containing early endosomes (50). Knock-down of VPS35 and M6PR also suppressed endocytosis of PrP^C, albeit less prominently. This suggests additional physical or epistatic interactions of these genes with PrP^C. Finally, knock-down of VPS28 resulted in an increased uptake of PrP^C by reducing PrP^C cell surface expression.

In summary, we provide proof-of-concept for FRET-based assays that are suited as high-throughput screening platforms to identify small molecules or compounds that genetically or pharmacologically block or induce PrP^C endocytosis. The assays can be utilized to measure the internalization rate, to characterize the different endocytosis pathways and to perform large-scale RNAi screenings to identify genes regulating PrP^C expression, biosynthesis and endocytosis. The knowledge gained from these experiments is likely to lead to the discovery of novel compounds for the treatment of prion diseases, and perhaps even for other protein misfolding and aggregation diseases which share pathways with those active in prion diseases.

EXPERIMENTAL PROCEDURES

Cell Culture — N2a PK1 (a subclone of neuroblastoma N2a cells) and Hpl $PrnP^{-/-}$ cells (21) were cultured in 75-cm^2 tissue culture flasks in OptiMEM medium supplemented with 10% (vol/vol) fetal bovine serum (FBS) and 1% penicillin/streptomycin. Human HeLa and A549 cells were cultured in DMEM medium supplemented with 10% (vol/vol) fetal bovine serum and 1% penicillin/streptomycin. In FRET experiments, all cell lines were cultured in medium without FBS, antibiotics and phenol red. To determine cell numbers and cell viability, resuspended cells were stained with trypan blue and counted in a Neubauer chamber.

FRET Antibody Labeling — Monoclonal POM antibodies were labeled in-house for FRET applications. The donor fluorophore was Europium chelate (Eu-W1024 ITC chelate, AD0096, PerkinElmer). Coupling to proteins occurs at alkaline pH via reaction of lysine residues and free N termini with the aromatic isothiocyanate group of the Europium chelate. To remove possible contaminant interfering with labeling, antibodies were dialyzed overnight in 1 ml of 100 mM sodium carbonate buffer (Na_2CO_3, pH 9-9.3). Dialysis cassettes (Slide-A-Lyzer®, Thermo scientific) with a 7 kDa cut-off were used. Dialysis was done under stirring in a volume of 2 l of 100 mM Na_2CO_3 pH 9-9.3 at 4°C overnight. Dialysis buffer was changed after 4-6 h.

Antibodies were concentrated by Centricon concentrators (Millipore). Protein concentration was adjusted by the Bradford or BCA assay to a concentration of about 5 mg/ml. A molar excess of 24x of Europium chelate over IgG was added into the protein solution on ice and incubated in 100 mM Na_2CO_3 over night at 4°C. Separation of the labeled protein from non-reacted chelate was performed by size exclusion chromatography (Superdex 200 column, GE Healthcare). Elution from column was done with 50 mM Tris-HCl pH 7.8 + 0.9% sodium chloride. Sample fractions of 500 μl were collected. Fractions were pooled and concentrated with Micron centrifugal filters (Amicon). Labeling ratio and concentration of labeled proteins were assessed by an Europium standard solution (Perkin Elmer) and NanoDrop measurement, respectively. Allophycocyanin (APC, AnaTagTM Labeling Kit 72111, Anaspec) was used as acceptor fluorophore for conjugation to POM antibodies. Maleimide groups of APC react with sulfhydryl groups on the target antibody to form a covalent bond. POM antibodies were

concentrated to 2-10 mg/ml in a volume of 100 µl with Centricon concentrators (Millipore). Antibodies were reduced with 20 µl dithiothreithol (DTT) per ml of IgG solution for 30 min without agitation at room temperature. Depending on reaction volume, reduced antibodies were desalted either by spin or gravity columns. Protein concentration was assessed by NanoDrop measurement. For the conjugation reaction, 1.5 mg of activated APC per mg reduced IgG was added to the reduced antibodies solution and incubated for 1 h at room temperature with agitation. Free thiol groups were blocked by adding DMSO and NEM for 30 min at room temperature. To remove free APC molecules from antibody solution, reaction mixture was purified via a protein G Sepharose column (Sigma). The column was washed with water and 10 volumes of 20 mM phosphate buffer pH 7 to equilibrate. Samples were added and washed with five volumes 20 mM phosphate buffer pH 7. Flow-through was collected. The column was eluted with 0.1 M glycine pH 2.3 and diluted with 1 M Tris HCl (pH 8). APC-labeled POM antibodies were characterized by NanoDrop (A280 and A650).

Time-resolved Fluorescence Measurements — The Wallac EnVision multilabel reader (PerkinElmer) was used for all FRET experiments using protocols installed by the manufacturer. A nitrogen laser device (337 nm) excites Eu which activates APC in a distance-dependent manner. Fluorescence emissions were monitored both at 615 nm for Eu and at 665 nm for APC. An integration time of 100 or 400 µs was used after a time delay ranging from 50 to 100 µs to remove short-lived background signals.

Data Analysis — The distance-dependent energy transfer between the chromophore-conjugated antibodies determines the FRET signal intensity in the presence of PrP and is henceforth reported as "net FRET" signal. Net FRET signals are the number of APC counts depending on FRET events and calculated by using the following equation:

$$NetFRETsignal = (counts - APC_{blank})_{APC} - P(counts - buffer)_{Eu}, \quad (1)$$

where counts are the raw FRET-dependent signals in APC and Eu channel, respectively, minus the background fluorescence. The proportionality factor P defines spectral overlap compensations and is measured by the equation:

$$P = \frac{(Eu_{blank} - buffer)_{APC}}{(Eu_{blank} - buffer)_{Eu}}. \quad (2)$$

Eu_{blank} and APC_{blank} correspond to all reagents except Eu or APC in Eu or APC channel, respectively. In addition, cells deficient of PrP were used as negative controls.

To show the reliability of FRET-based immunoassays for high-throughput applications, the statistical parameter Z' factor (22) was calculated by the formula:

$$Z' = 1 - \frac{3 * SD_{pos} + 3 * SD_{neg}}{|\mu_{pos} - \mu_{neg}|} \quad (3)$$

where SD is the standard deviation and µ is the mean of positive and negative controls. An assay is considered to be excellent for high-throughput applications if the Z' factor is equal or superior to 0.5.

PrP Cell Surface FRET Assay — Cells were plated one day before into 96-well or 384-well microtiter plates (Perkin Elmer) in cell culture medium without phenol red at the desired density. Cells were washed once and FRET antibody labeling was performed at 4°C containing 1 nM Eu-labeled and 5 nM APC-labeled antibodies in Tris-/Krebs buffer (20 mM Tris pH 7.4, 118 mM NaCl, 5.6 mM glucose, 1.2 mM KH_2PO_4, 1.2 mM $MgSO_4$, 4.7 mM KCl, 1.8 mM $CaCl_2$, 1% BSA). FRET signals were measured with the Wallac EnVision reader (homogeneous time-resolved (TR)-FRET assay) with a time delay of approximately 100 µ seconds between the excitation and fluorescence measurement. Thereafter, plates were washed with Tris-/Krebs buffer and the FRET signal was measured again (TR-FRET assay). Pharmacological treatment of cells was performed with brefeldin A diluted in DMSO, for 18 h incubation at 37°C. DMSO concentration was kept constant at 0.75%. Cells were washed once with ice-cold Tris-/Krebs buffer and labeled with FRET antibodies as mentioned above. Enzymatic treatment of cells was done with PI-PLC. PI-PLC was

dialyzed in PBS overnight and protein concentration was assessed by the Bradford assay (BioRad). Digestion was carried out either at 4°C or at 37°C for 1 h during shaking (450 rpm). Supernatant was transferred into a new plate and medium and cells were labeled with FRET antibodies. The neuronal Hpl $PrnP^{-/-}$ cell line was used as negative control for assay development and optimization.

PrP Endocytosis FRET Assay — Cells were plated and cultured for one day in 96- or 384-well microtiter plates (Perkin Elmer) at the desired density. Cells were washed once and labeled with 1 nM Eu-labeled POM antibodies in Tris-/Krebs buffer for 30 min at 4°C. After washing out unbound antibodies, cells were pre-incubated for 5 minutes at 37°C. At different time intervals, 5 nM of APC-labeled antibodies were added in cell culture medium without phenol red. FRET signals were measured with a Wallac EnVision reader in the homogeneous FRET assay mode or after a washing step in the TR-FRET mode. The internalization rate of PrP^C was calculated with the following equation:

$$Uptake = \frac{(FRETPrP^C_{t=0}) - (FRETPrP^C_{t=x})}{(FRETcellsurfacePrP^C{}_{t=0})} \quad (4)$$

To suppress PrP^C endocytosis, A549 cells were treated with ascending doses of chlorpromazine (CPZ) or methyl-beta-cyclodextrin (MbetaCD), and subsequently labeled with POM2-Eu. After 30 min of incubation at 37°C POM2-APC was added and inhibition of PrP^C uptake was assayed by TR-FRET.

siRNA Treatment — To transfect siRNA into mammalian cells, LipofectamineTM 2000 (InvitrogenTM) was utilized. One day before transfection, 2500 cells in 80 µl DMEM cell culture medium without antibiotics were seeded into a 96-well plate per well. SiRNA:LipofectamineTM 2000 complexes were prepared as follows: 5 µl siRNA (1 µM) was diluted in 5 µl pre-warmed DMEM cell culture medium without serum and antibiotics and mixed gently. 0.1 µl LipofectamineTM 2000 was diluted in 9.9 µl pre-warmed DMEM cell culture medium without serum and antibiotics. After an incubation of 5 min at room temperature, the diluted LipofectamineTM 2000 was combined with the diluted siRNA. To allow formation of siRNA:LipofectamineTM 2000 complexes, the combined solutions were mixed and incubated for 20 min at room temperature. 20 µl of siRNA:LipofectamineTM 2000 complexes were added to each well of the 96-well plate and cells were cultured at 37°C in a CO_2 incubator for 72 h.

Quantitative PCR — Cell cultures were prepared and incubated as stated above. Cells were washed once with PBS and total RNA was extracted using the RNeasy® mini kit (Qiagen) according to the manufacturer's protocol. RNA concentration and purity was determined by NanoDrop measurements. cDNA was synthesized from 0.5 µg total RNA with QuantiTect reverse transcription kit (Qiagen) using random hexamers according to the manufacturer's protocol. Before cDNA synthesis, genomic DNA was eliminated. Successful cDNA synthesis and contamination of total RNA with genomic DNA was tested by PCR with primer specific for GAPDH. Quantitative real-time PCR was performed using the SYBR Green master mix (Applied Biosystems) on an ABI Prism VIIA7 sequence detector (PerkinElmer). Fold regulation was calculated relative to untreated cells after normalization to the GAPDH signal. The following primer pairs were used: VPS28 sense (NM_16208): 5'–TTG TTC CCA GGG GCT CCT AT-3', antisense: 5'–ATC TTC CCG ACC GCG AG-3'. RAB5A sense (NM_004162): 5'-TTA GAA AAG CAG CCC CAA TG-3', antisense 5'-GTA CTT CTG GGA GAG TCC GC-3'. AP2M1 sense (NM_004068): 5'-AAT CAT GGC GGC AGA TCA GT-3', sense 5'-ATC TTG GGA TCC GGA GAG TG-3'. GIT2 sense (NM_014776): 5'- AGA CAA ATC CAG GCT GCT GT-3', antisense 5'-GCG CCT CGT GGA AAT ACA GT-3'. EHD1 sense (NM_006795): 5'-AAG AGC AGG ATG ATG CGG T-3', antisense 5'-CCT GTC TGG AGA GAA GCA GC-3'. M6PR sense (NM_002355): 5'-ATT CTC TCA CTG CCA CAG CC-3', antisense 5'-TGG CTA CTC CAG TTT CCC AC-3'. VPS35 sense (NM_018206): 5'-CAC TGA TAG TCT GGT GGG CA-3', antisense 5'-CAG CTT ACC AGC TGG CTT TT-3'. PRNP sense (NM_000311): 5'-AGT GTT CCA TCC TCC AGG C-3', antisense 5'-GAG CTT CTC CTC TCC TCA CG-3'. GAPH sense (NM_002046): 5'-CAT GAG AAG TAT GAC AAC AGC CT, antisense 5'-AGT CCT TCC ACG ATA CCA AA GT-3'.

Cell Viability Assay — The alamarBlue® assay (Invitrogen) was utilized to assess cell viability according to the manufacturer's protocol. All experiments were performed in cell culture medium without antibiotics and phenol red. Cells were incubated with the alamarBlue dye at 37°C and the fluorescence intensity was measured with a plate reader after 1-6 hrs.

Acknowledgments: We thank Irina Abakumova and Clemence Tournaire for technical help. AA is the recipient of an Advanced Grant of the European Research Council, a European Union Framework 7 Grant (NEURINOX), the Swiss National Foundation, the Clinical Research Priority Programs "Small RNAs" and "Human Hemato-Lymphatic Diseases", the Swiss Initiative in Systems Biology, SystemsX.ch (PrionX, SynucleiX), and the Novartis Research Foundation. SH is the recipient of the Swiss Initiative in Systems Biology, SystemsX.ch (SynucleiX) and the commission innovations of the University Hospital of Zurich. LP is the recipient of a Consolidator Grant of the Swiss National Science Foundation, the University of Zurich Research Priority Program in Systems Biology, and the Swiss Initiative in Systems Biology, SystemsX.ch (LipidX, PrionX). PL is the recipient of the Swiss National Science Foundation (*PP*00*P*3_157531).

Conflict of interest: The authors declare that they have no conflicts of interest with the contents of this article.

Author contributions: BAB designed, performed, analyzed the experiments and wrote the initial draft of the paper. RM provided technical assistance. PL, LP designed the experiments. SH and AA conceived, coordinated and designed the study, analyzed data and wrote the paper. All authors analyzed and reviewed the results and approved the final version of the manuscript.

REFERENCES

1. Aguzzi, A. and Calella, A, M. (2009) Prions: protein aggregation and infectious diseases, *Physiol Rev.* **89**(4), 1105–52.
2. Prusiner, S, B. (2004) *Prion biology and diseases* volume 1050, Cold spring harbor laboratory press New York
3. Prusiner, S, B., Scott, M, R., DeArmond, S, J., and Cohen, F, E. (1998) Prion protein biology, *Cell* **93**(3), 337–348.
4. Taylor, D, R. and Hooper, N, M. (2007) The low-density lipoprotein receptor-related protein 1 (lrp1) mediates endocytosis of the cellular prion protein, *Biochem. J.* **402**(1), 17–23.
5. Shyng, S, L., Huber, M, T., and Harris, D, A. (1993) A prion protein cycles between cell surface and an endocytic compartment in cultured neuroblastoma cells, *J Biol Chem* **268**(21), 15922–8.
6. Harris, D, A. (2003) Trafficking, turnover and membrane topology of prp, *Br Med Bull.* **66**, 71–85.
7. Prado, M, A., Alves-Silva, J., Magalhâes, A, C., Prado, V, F., Linden, R., Martins, V, R., and Brentani, R, R. (2004) Prpc on the road: trafficking of the cellular prion protein, *J Neurochem.* **88**(4), 769–81.
8. Campana, V., Sarnataro, D., and Zurzolo, C. (2005) The highways and byways of prion protein trafficking, *Trends Cell Biol* **15**(2), 102–11.
9. Shyng, S, L., Lehmann, S., Moulder, K, L., and Harris, D, A. (1995) Sulfated glycans stimulate endocytosis of the cellular isoform of the prion protein, prpc, in cultured cells, *J Biol Chem* **270**(50), 30221–9.
10. Sunyach, C., Jen, A., Deng, J., Fitzgerald, K, T., Frobert, Y., Grassi, J., McCaffrey, M, W., and Morris, R. (2003) The mechanism of internalization of glycosylphosphatidylinositol-anchored prion protein, *EMBO J* **22**(14), 3591–601.
11. Taylor, D, R., Watt, N, T., Perera, W, S., and Hooper, N, M. (2005) Assigning functions to distinct regions of the n-terminus of the prion protein that are involved in its copper-stimulated, clathrin-dependent endocytosis, *J Cell Sci* **118**(Pt 21), 5141–53.
12. Morrison, L, E. (1988) Time-resolved detection of energy transfer: theory and application to immunoassays, *Anal Biochem.* **174**(1), 101–20.
13. Jares-Erijman, E, A. and Jovin, T, M. (2003) Fret imaging, *Nat Biotechnol* **21**(11), 1387–95.
14. PR, S. (2000) The renaissance of fluorescence resonance energy transfer, *Nat Struct Biol* **7**(9), 730–4.
15. Bazin, H., Trinquet, E., and Mathis, G. (2002) Time resolved amplification of cryptate emission: a versatile technology to trace biomolecular interactions, *J Biotechnol* **82**(3), 233–50.
16. Polymenidou, M., Moos, R., Scott, M., Sigurdson, C., Shi, Y, Z., Yajima, B., Hafner-Bratkovic, I., Jerala, R., Hornemann, S., Wuthrich, K., Bellon, A., Vey, M., Garen, G., James, M, N., Kav, N., and Aguzzi, A. (2008) The pom monoclonals: a comprehensive set of antibodies to non-overlapping prion protein epitopes, *PLoS One* **3**(12), –.
17. Bolton, D, C., Seligman, S, J., Bablanian, G., Windsor, D., Scala, L, J., Kim, K, S., Chen, C, M., Kascsak, R, J., and Bendheim, P, E. (1991) Molecular location of a species-specific epitope on the hamster scrapie agent protein, *J Virol* **65**(7), 3667–75.
18. Hornemann, S., Korth, C., Oesch, B., Riek, R., Wider, G., Wüthrich, K., and Glockshuber, R. (1997) Recombinant full-length murine prion protein, mprp(23-231): purification and spectroscopic characterization, *FEBS Lett* **413**(2), 277–81.
19. Riek, R., Hornemann, S., Wider, G., Billeter, M., Glockshuber, R., and Wüthich, K. (1996) Nmr structure of the mouse prion protein domain prp(121-231), *Nat.* **382**(6587), 180–2.
20. Wüthrich, K. and Riek, R. (2001) Three-dimensional structures of prion proteins, *Adv Protein Chem* **57**, 55–82.
21. Sakudo, A., Onodera, T., and Ikuta, K. (2007) Prion protein gene-deficient cell lines: powerful

tools for prion biology, *Microbiol Immunol* **51**(1), 1–13.
22. Zhang, J, H., Chung, T, D., and Oldenburg, K, R. (1999) A simple statistical parameter for use in evaluation and validation of high throughput screening assays, *J Biomol Screen* **4**(2), 67–73.
23. Aguzzi, A. and Polymenidou, M. (2004) Mammalian prion biology: one century of evolving concepts, *Cell* **116**(2), 313–27.
24. Nebenführ, A., Ritzenthaler, C., and Robinson, D, G. (2002) Brefeldin a: deciphering an enigmatic inhibitor of secretion, *Plant Physiol* **130**(3), 1102–8.
25. Vercauteren, D., Vandenbroucke, R., Jones, A, T., Rejman, J., Demeester, J., De Smedt, S, C., Sanders, N, N., and Braeckmans, K. (2010) The use of inhibitors to study endocytic pathways of gene carriers: optimization and pitfalls, *Mol Ther* **18**(3), 561–9.
26. Wang, L, H., Rothberg, K, G., and Anderson, R, G. (1993) Mis-assembly of clathrin lattices on endosomes reveals a regulatory switch for coated pit formation, *J Cell Biol* **123**(5), 1107–17.
27. Klein, U., Gimpl, G., and Fahrenholz, F. (1995) Alteration of the myometrial plasma membrane cholesterol content with beta-cyclodextrin modulates the binding affinity of the oxytocin receptor. biochemistry, *Biochem.* **34**(42), 13784–93.
28. Luo, K., Li, S., Xie, M., Wu, D., Wang, W., Chen, R., Huang, L., Huang, T., Pang, D., and Xiao, G. (2010) Real-time visualization of prion transport in single live cells using quantum dots, *Biochem. Biophys Res Commun* **394**(3), 493–7.
29. Rodal, S, K., Skretting, G., Garred, O., Vilhardt, F., van Deurs, B., and K, S. (1999) Extraction of cholesterol with methyl-beta-cyclodextrin perturbs formation of clathrin-coated endocytic vesicles, *Mol Biol Cell* **10**(4), 961–74.
30. Sarnataro, D., Caputo, A., Casanova, P., Puri, C., Paladino, S., Tivodar, S, S., Campana, V., Tacchetti, C., and Zurzolo, C. (2009) Lipid rafts and clathrin cooperate in the internalization of prp in epithelial frt cells, *PLoS One* **4**(6), –.
31. Lanzetti, L., Rybin, V., Malabarba, M, G., Christoforidis, S., Scita, G., Zerial, M., and Di Fiore, P, P. (2000) The eps8 protein coordinates egf receptor signalling through rac and trafficking through rab5, *Nat.* **408**(6810), 374–7.
32. Martinu, L., Santiago-Walker, A., Qi, H., and Chou, M, M. (2002) Endocytosis of epidermal growth factor receptor regulated by grb2-mediated recruitment of the rab5 gtpase-activating protein rn-tre, *J Biol Chem* **277**(52), 50996–1002.
33. McLauchlan, H., Newell, J., Morrice, N., Osborne, A., West, M., and Smythe, E. (1998) A novel role for rab5-gdi in ligand sequestration into clathrin-coated pits, *Curr Biol* **8**(1), 34–45.
34. Stenmark, H., Valencia, A., Martinez, O., Ullrich, O., Goud, B., and Zerial, M. (1994) Distinct structural elements of rab5 define its functional specificity, *EMBO J* **13**(3), 575–83.
35. Boucrot, E., Saffarian, S., Zhang, R., and Kirchhausen, T. (2010) Roles of ap-2 in clathrin-mediated endocytosis, *PLoS One* **5**(5), –.
36. Le Borgne, R. and Hoflack, B. (1997) Mannose 6-phosphate receptors regulate the formation of clathrin-coated vesicles in the tgn, *J Cell Biol* **137**(2), 335–45.
37. Bonifacino, J, S. and Hurley, J, H. (2008) Retromer, *Curr Opin Cell Biol* **20**(4), 427–36.
38. Dhungel, N., Eleuten, S., Li, L., Kramer, N, J., Chartron, J, W., Spencer, B., Kosberg, K., Fields, J, A., Stafa, K., Adame, A., Lashuel, H., Frydman, J., Shen, K., Masliah, E., and Gitler, A. (2015) Parkinson's disease genes vps35 and eif4g1 interact genetically and converge on alpha - synuclein, *Neuron* **85**(1), 76–87.
39. Rainey, M, A., George, M., Ying, G., Akakura, R., Burgess, D, J., Siefker, E., Bargar, T., Doglio, L., Crawford, S, E., Todd, G, L., Govindarajan, V., Hess, R, A., Band, V., Naramura, M., and Band, H. (2010) The endocytic recycling regulator ehd1 is essential for spermatogenesis and male fertility in mice, *BMC Dev Biol* **10**(37), 328–42.
40. Bishop, N. and Woodman, P. (2001) Tsg101/mammalian vps23 and mammalian vps28 interact

directly and are recruited to vps4-induced endosomes, *J Biol Chem* **276**(15), 11735–42.

41. Premont, R, T., Perry, S, J., Schmalzigaug, R., Roseman, J, T., Xing, Y., and Claing, A. (2004) The git/pix complex: an oligomeric assembly of git family arf gtpase-activating proteins and pix family rac1/cdc42 guanine nucleotide exchange factors, *Cell Signal* **16**(9), 1001–11.
42. Brandner, S., Isenmann, S., Raeber, A., Fischer, M., Sailer, A., Kobayashi, Y., Marino, S., Weissmann, C., and Aguzzi, A. (1996) Normal host prion protein necessary for scrapie-induced neurotoxicity, *Nat.* **379**(6563), 339–43.
43. Sonati, T., Reimann, R, R., Falsig, J., Baral, P, K., O'Connor, T., Hornemann, S., Yaganoglu, S., Li, B., Herrmann, U, S., Wieland, B., Swayampakula, M., Rahman, M, H., Das, D., Kav, N., Riek, R., Liberski, P, P., James, M, N., and A, A. (2013) The toxicity of antiprion antibodies is mediated by the flexible tail of the prion protein, *Nat.* **501**(7465), 102–6.
44. Heppner, F, L., Musahl, C., Arrighi, I., Klein, M, A., Rülicke, T., Oesch, B., Zinkernagel, R, M., Kalinke, U., and A, A. (2001) Prevention of scrapie pathogenesis by transgenic expression of anti-prion antibodies, *Sci.* **294**(5540), 178–82.
45. Pfeifer, A., Eigenbrod, S., Al-Khadra, S., Hofmann, A., Mitteregger, G., Moser, M., Bertsch, U., and Kretzschmar, H. (2006) Lentivector-mediated rnai efficiently suppresses prion protein and prolongs survival of scrapie-infected mice, *J Clin Invest* **116**(12), 3204–10.
46. Karapetyan, Y, E., Sferrazza, G, F., Zhou, M., Ottenberg, G., Spicer, T., Chase, P., Fallahi, M., Hodder, P., Weissmann, C., and Lasmézas, C, I. (2013) Unique drug screening approach for prion diseases identifies tacrolimus and astemizole as antiprion agents, *Proc Natl Acad Sci* **110**(17), 7044–9.
47. Triantaphyllidou, I, E., Sklaviadis, T., and Vynios, D, H. (2006) Detection, quantification, and glycotyping of prion protein in specifically activated enzyme-linked immunosorbent assay plates, *Anal Biochem.* **359**(2), 176–82.
48. Maurel, D., Kniazeff, J., Mathis, G., Trinquet, E., Pin, J, P., and Ansanay, H. (2004) Cell surface detection of membrane protein interaction with homogeneous time-resolved fluorescence resonance energy transfer technology, *Anal Biochem.* **329**(2), 253–62.
49. Marella, M., Lehmann, S., Grassi, J., and Chabry, J. (2002) Filipin prevents pathological prion protein accumulation by reducing endocytosis and inducing cellular prp release, *J Biol Chem* **277**(28), 25457–64.
50. Magalhães, A, C., Silva, J, A., Lee, K, S., Martins, V, R., Prado, V, F., Ferguson, S, S., Gomez, M, V., Brentani, R, R., and Prado, M, A. (2002) Endocytic intermediates involved with the intracellular trafficking of a fluorescent cellular prion protein, *J Biol Chem* **277**, 33311–8.

TABLES

	Hpl $PrnP^{-/-}$	0.25 ng/ml	0.5 ng/ml	1 ng/ml	2 ng/ml	4 ng/ml	8 ng/ml	16 ng/ml	32 ng/ml	64 ng/ml	128 ng/ml
%CV	13.24	12.20	8.14	33.31	11.41	4.70	9.55	6.86	2.14	5.28	8.16
S/N		2.59	4.66	1.96	6.31	16.20	9.11	12.94	37.59	17.06	11.25
Z'		< 0.5	< 0.5	< 0.5	< 0.5	0.75	0.62	0.73	0.89	0.79	0.70

	Hpl $PrnP^{-/-}$	2 µg/ml	4 µg/ml	8 µg/ml	16 µg/ml	32 µg/ml	64 µg/ml	128 µg/ml	256 µg/ml	512 µg/ml	1024 µg/ml
%CV	37.69	35.63	40.17	37.65	30.59	17.77	14.05	10.94	9.62	7.87	6.71
S/N		-0.09	-0.15	-0.01	0.90	1.40	2.50	3.43	5.49	7.91	10.76
Z'		< 0.5	< 0.5	< 0.5	< 0.5	< 0.5	< 0.5	< 0.5	< 0.5	< 0.5	0.61

Table 1: Performance of the homogeneous FRET assay for recPrP (upper table) and PrP^C from murine N2aPK1 cell lysates (lower table). The assay was evaluated according to three parameters: coefficient of variation (%CV), signal-to-noise ratio (S/N) and the Z' factor. Acceptable values were: %CV values < 10%, S/N > 8 and Z' > 0.5.

HTRF	32K	16K	8K	4K	2K	1K	0.5K	0.25K	0.13K	0.06K	0K
%CV	3.407	3.120	5.056	3.152	3.244	2.071	6.239	4.921	4.638	8.126	3.863
S/N	8.34	7.25	4.54	5.66	4.35	3.86	1.46	0.19	0.87	-0.18	0.00
Z'	0.53	< 0.5	< 0.5	< 0.5	< 0.5	< 0.5	< 0.5	< 0.5	< 0.5	< 0.5	< 0.5

TR	32K	16K	8K	4K	2K	1K	0.5K	0.25K	0.13K	0.06K	0K
%CV	13.02	7.216	6.609	7.330	7.043	16.54	11.19	23.16	47.96	64.86	82.06
S/N	7.59	13.66	14.89	13.42	13.77	5.83	7.73	3.50	1.63	1.01	0.00
Z'	0.58	0.76	0.78	0.75	0.75	< 0.5	< 0.5	< 0.5	< 0.5	< 0.5	< 0.5

HTRF	32K	16K	8K	4K	2K	1K	0.5K	0.25K	0.13K	0.06K	0K
%CV	2.421	1.114	3.400	7.895	2.051	5.153	5.177	2.767	11.97	3.086	3.863
S/N	22.0	30.3	12.9	4.63	9.29	3.69	1.15	0.95	-0.72	-2.16	0.00
Z'	0.81	0.86	0.69	< 0.5	0.54	< 0.5	< 0.5	< 0.5	< 0.5	< 0.5	< 0.5

TR	32K	16K	8K	4K	2K	1K	0.5K	0.25K	0.13K	0.06K	0K
%CV	8.190	5.421	5.856	11.18	7.243	8.366	23.43	63.48	64.15	62.31	82.11
S/N	11.9	16.9	14.2	7.71	6.67	3.69	1.54	0.58	-0.06	0.14	0.00
Z'	0.70	0.77	0.71	< 0.5	< 0.5	< 0.5	< 0.5	< 0.5	< 0.5	< 0.5	< 0.5

Table 2: Assay performance of the cell surface FRET assay in the HTRF mode (without washing steps) and TR-FRET mode (after washing) in A549 (upper tables) and HeLa cells (lower tables) was assessed by three parameters: coefficient of variation (%CV), signal-to-noise ratio (S/N) and the Z' factor. Acceptable values were: %CV values < 10%, S/N > 8 and Z' > 0.5. K: cell number in thousands.

Abbreviation	Description
AP2M1	Encodes the adaptor protein 2 (AP-2) which is involved in clathrin-dependent endocytosis
EHD1	Encodes the EH domain-containing protein 1, plays a role in endocytosis
GIT2	Encodes the ARF GTPase-activating protein GIT2
M6PR	Encodes the mannose 6-phosphate receptor, interacts with AP1 clathrin adaptor complex
RAB5A	G-protein, required for the fusion of plasma membrane and early endosomes
VPS28	Encodes the vacuolar protein sorting-associated protein 28 homolog, involved in endosomal sorting of cell surface receptors
VPS35	Encodes the vacuolar protein sorting-associated protein 35 homolog, involved in retrograde transport of proteins from endosomes to the trans-Golgi network

Table 3: Overview of the tested siRNAs on PrP^C endocytosis rate and cell surface level. For the study of PrP^C endocytosis and cell surface expression, seven siRNAs acting in protein recycling pathways and their downstream organelles were selected.

	PrP^C cell surface expression		PrP^C endocytosis	
	mean ± SD (t0)	normalized to untreated (t0)	mean ± SD (t0-t30)	endocytosis rate
untreated	448.43 ± 103.37	1 ± 0.23	213.62 ± 110.26	0.48 ± 0.36
PrP	229.24 ± 108.70	0.51 ± 0.24	52.65 ± 118.97	0.23 ± 0.63
AP2M1	443.52 ± 19.41	0.99 ± 0.04	40.64 ± 30.35	0.09 ± 0.07
EHD1	493.18 ± 28.72	1.10 ± 0.06	254.44 ± 80.13	0.52 ± 0.19
GIT2	459.97 ± 50.50	1.03 ± 0.11	228.70 ± 90.94	0.50 ± 0.25
M6PR	435.74 ± 82.25	0.97 ± 0.18	79.65 ± 102.08	0.18 ± 0.27
RAB5A	202.00 ± 89.66	0.45 ± 0.20	-51.60 ± 115.41	-0.26 ± 0.46
VPS28	349.60 ± 125.23	0.78 ± 0.28	199.25 ± 136.61	0.57± 0.59
VPS35	344.96 ± 122.54	0.77 ± 0.27	65.19 ± 137.30	0.19 ± 0.47

Table 4: Effect of siRNA treatment on PrP^C cell surface expression and endocytosis rate. Left columns: Influence of siRNA treatment on PrP^C cell surface expression. Cells were incubated for three days with siRNAs. PrP^C cell surface level was detected with the POM2-Eu/POM2-APC antibody pair. PrP^C cell surface expression of siRNA treated cells is expressed as fold of untreated cells . Right columns: Influence of siRNA treatment on the endocytosis rate of PrP^C. Cells were incubated for three days with siRNAs and labeled with POM2-Eu at 4 ºC. To induce endocytosis, cells were exposed to 37 ºC. At time point t0 = 0 min and t1 = 30 min POM2-APC was added. The endocytosis rate was calculated as described in "experimental procedures".

FIGURES

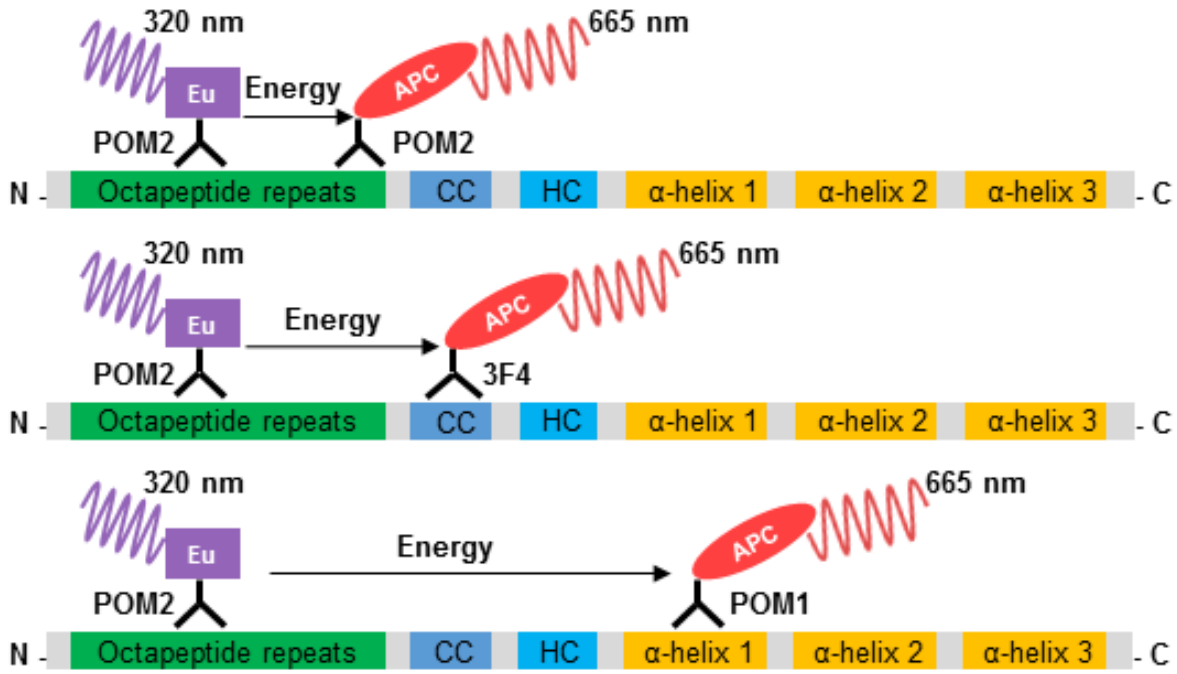

Figure 1: Schematic representation of the antibody binding sites for PrP detection in the homogeneous TR-FRET assay. The assay is based on the in-solution binding of two fluorophore-labeled POM antibodies to identical or unique epitopes on PrP. POM antibodies were either labeled with Europium chelate (Eu) donor fluorophore or APC-labeled acceptor. The antibody pairs POM2-Eu/POM2-APC (upper) POM2-Eu/3F4-APC (middle) and POM2-Eu/POM1-APC (lower) were used in the assays. POM1 binds to alphahelix 1 in the C-terminal globular domain, POM2 to the octapeptide repeats (residues 51-91, mouse sequence) in the unfolded N-terminal part of PrP and 3F4 to the charged cluster (CC). The close proximity of the donor and acceptor antibodies upon binding to PrP leads to a fluorescent TR-FRET signal at 665 nm after excitation at 320 nm, which is proportional to the PrP concentration. HC: hydrophobic core region.

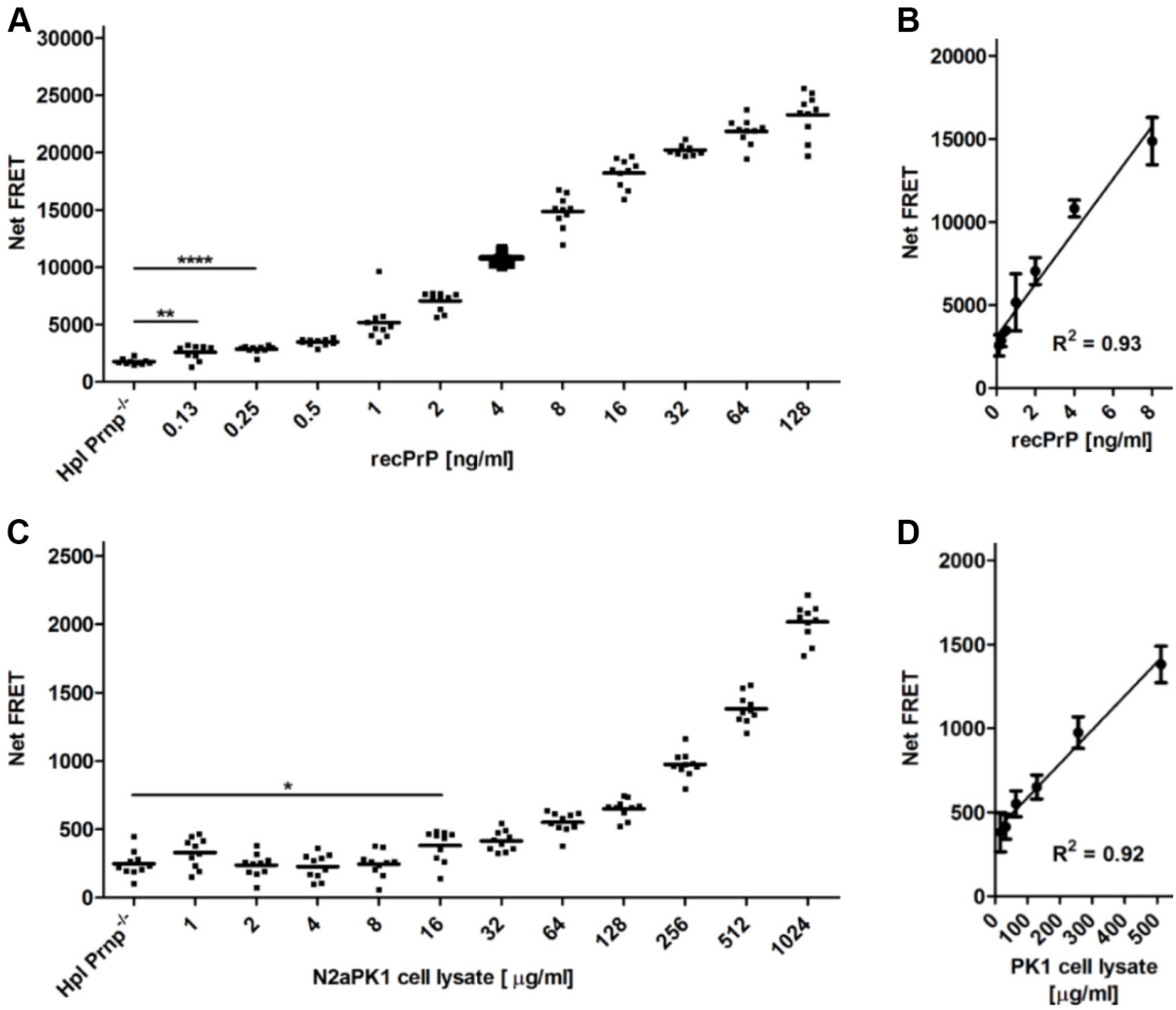

Figure 2: TR-FRET immunoassays for the detection of recombinant PrP and PrP^C in crude cell lysates. (A) Dilution range of recPrP using the antibody tandem pair POM1-Eu/POM2-APC. Recombinant PrP (128 - 0.125 ng/ml) was serially diluted in 1 mg/ml Hpl PrnP$^{-/-}$ cell lysate in polystyrene 384-well microtiter plates and detected by TR-FRET. The sensitivity (lower detection limit, LDL) of the assay is < 0.125 ng/ml. (B) Dynamic range of recPrP detection. The assay shows high linearity (R^2 = 0.93) at concentrations of 0.5-8 ng/ml for the detection of recPrP. (C) Dilution range of PrP^C in murine N2aPK1 cell lysates using the antibody pair POM1-Eu/POM2-APC. Cells were lysed in RIPA buffer and serially diluted (1024 - 1 µg/ml) in 1 mg/ml Hpl PrnP$^{-/-}$ cell lysate detected by TR-FRET. The sensitivity (lower detection limit, LDL) of the assay is < 20 µg/ml of crude cell extract. (D) Dynamic range of PrP^C detection. The assay shows a high linearity (R^2 = 0.92) in a concentration range between 500 to 30 µg/ml for the detection of PrP^C. Each dilution was performed in 10 replicate measurements (decuplicates). Error bars in the linear regression blots represent the standard deviation (± SD) of 6 replicate measurements. Student's t test: *: $p < 0.05$; **: $p < 0.01$; ***: $p < 0.001$; ****: $p < 0.0001$.

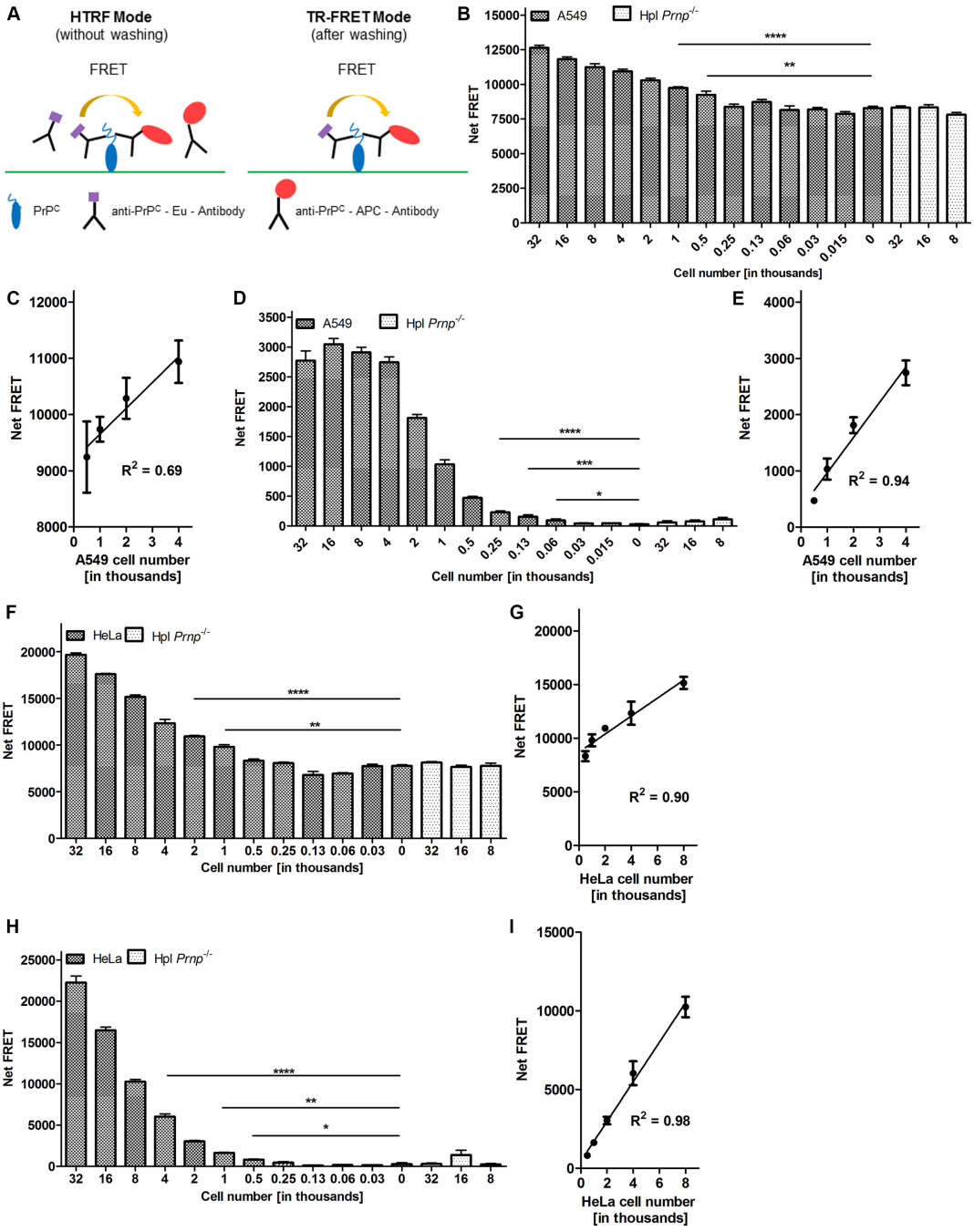

Figure 3: FRET immunoassay for the detection of PrP^C on the cell surface of intact human cells. (A) Schematic representation of the cell surface PrP^C FRET detection assay. The FRET signal was assessed either in the HTRF mode or after a washing step (TR-FRET mode) to remove unbound chromophore labeled antibodies. (B and F) Cell number dilution range in HTRF mode. A549 and HeLa cells were serially diluted (sextuplicates) in DMEM medium starting from 32'000 to 15 cells/well in polystyrene 384-well microtiter plates. Hpl PrnP$^{-/-}$ cells were used as negative controls. (C and G) Linear range of PrP^C cell surface detection of A549 and HeLa cells in the HTRF mode, respectively. (D and H) Cell number dilution range of A549 and HeLa cells in TR-FRET mode. (E and I) Linear range of PrP^C cell surface detection of A549 and HeLa cells in the TR-FRET mode, respectively. Error bars represent the standard deviation (± SD) of 6 replicate measurements. Student's t test: *: $p < 0.05$; **: $p < 0.01$; ***: $p < 0.001$; ****: $p < 0.0001$.

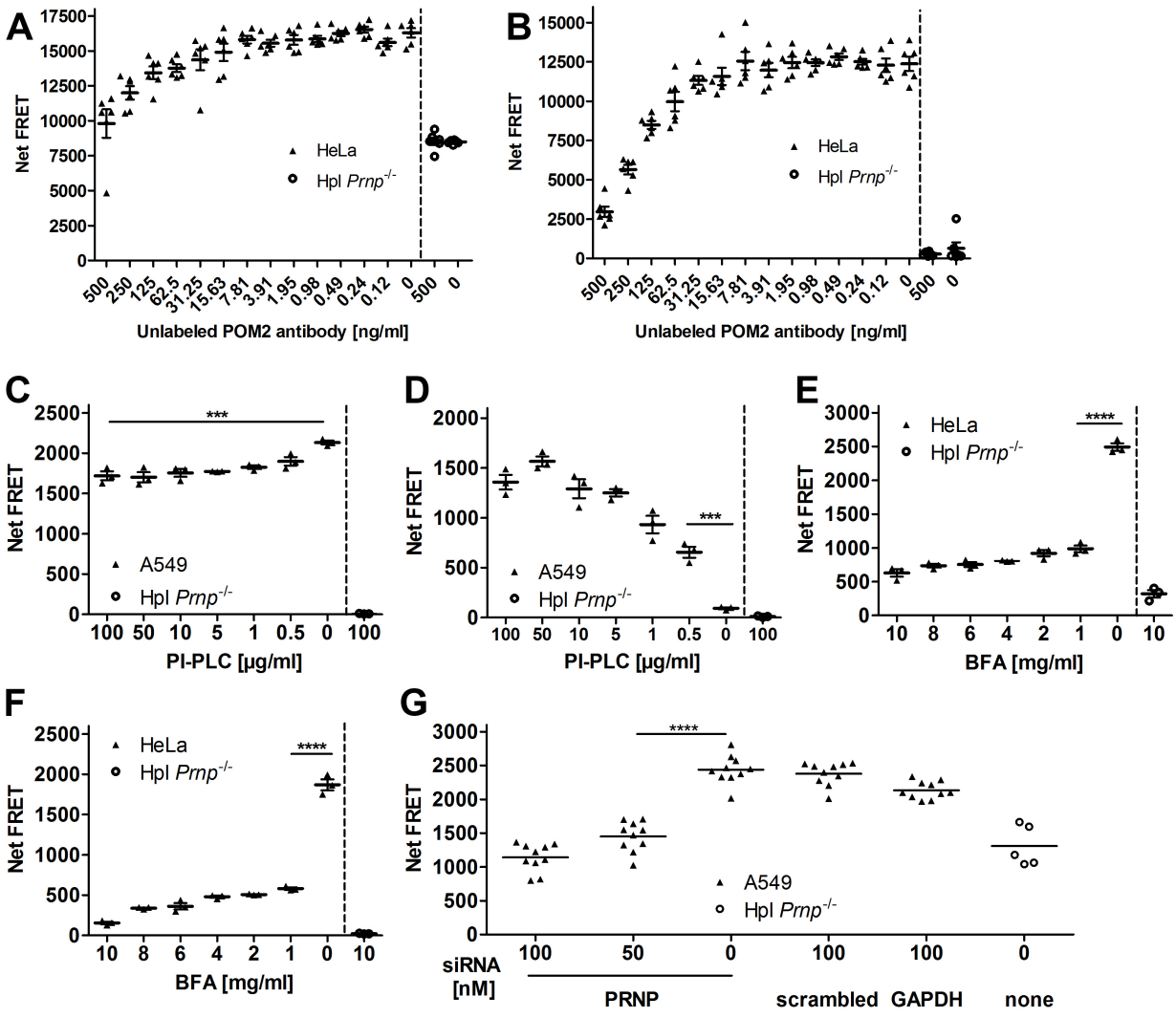

Figure 4: Suitability test of the FRET immunoassay for the manipulation of PrP cell surface expression. (A) Saturation binding curves of PrP^C. A constant number of HeLa cells was incubated with unlabeled POM2 antibody at different concentrations, followed by FRET signal detection with POM2-Eu/POM2-APC in HTRF mode. (B) Saturation binding curves of PrP^C after removing unbound POM-2 antibodies (TR-FRET mode). (C-D) Release of cell surface PrP^C by PI-PLC treatment. A constant number of A549 cells was labeled with POM2-Eu/POM2-APC followed by PI-PLC digestion at various concentrations. PrP^C cell surface FRET signal was measured after PI-PLC treatment at the cell surface (C) as well as in the cell culture medium (D). (E) Inhibition of PrP^C cell surface expression by BFA treatment. A constant number of HeLa cells was exposed to different BFA concentrations. PrP^C cell surface expression was measured by POM2-Eu/POM2-APC in the HTRF. (F) Same as (E), but in the TR-FRET mode. (G) siRNA mediated PRNP knockdown. A549 cells were treated with different concentrations of PRNP siRNA and control siRNAs for 3 days. PrP^C cell surface expression was detected with the POM2-Eu/3F4-APC FRET antibody pair. Scrambled and GAPDH siRNAs as well as Hpl PrnP$^{-/-}$ cells were used as negative and positive controls, respectively. Error bars represent the standard deviation (± SD) of 6 replicate measurements. Student's t test: *: $p < 0.05$; **: $p < 0.01$; ***: $p < 0.001$; ****: $p < 0.0001$.

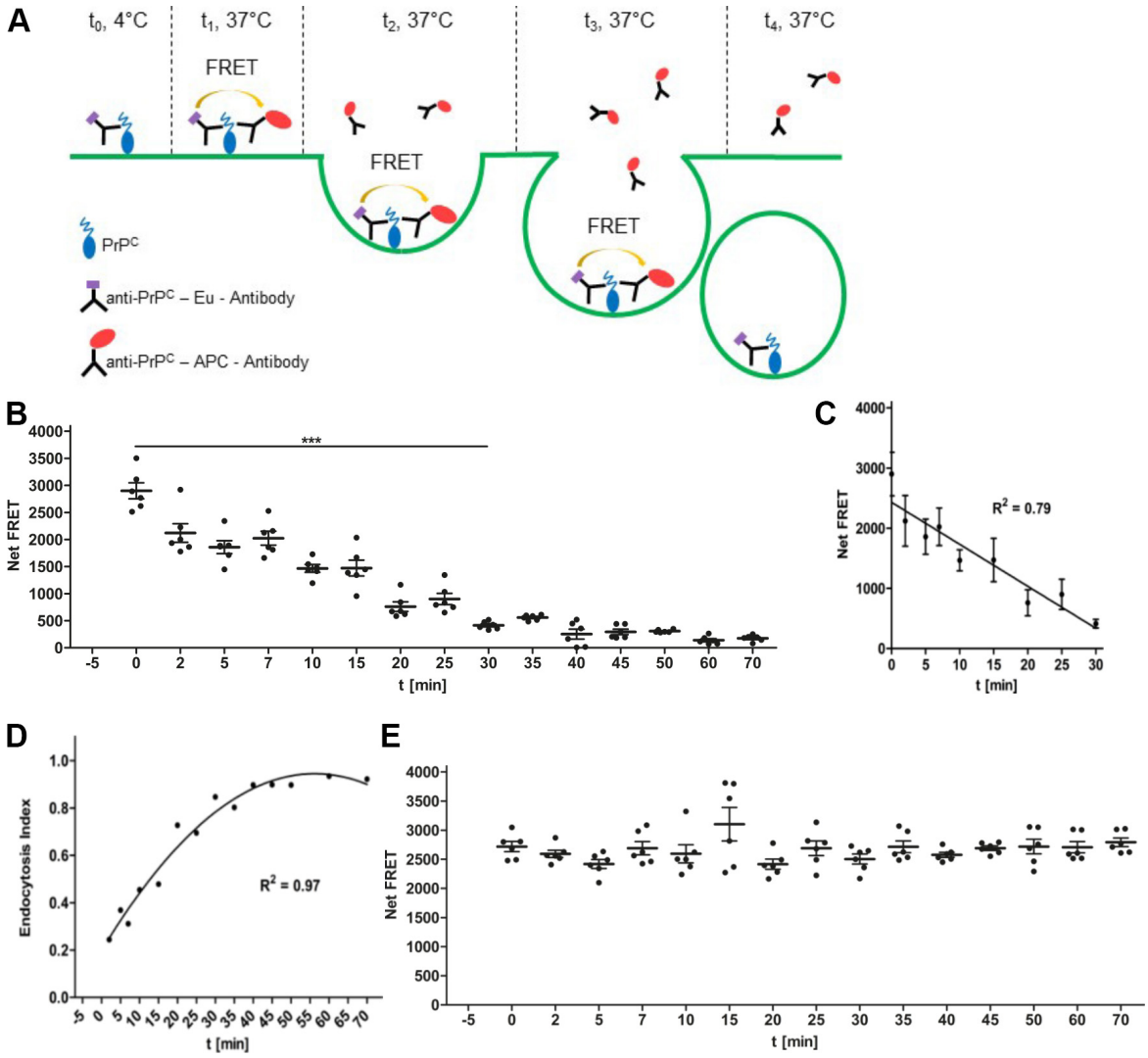

Figure 5: Principle of the endocytosis FRET immunoassay and detection of PrP^C uptake by human cells. (A) Schematic representation of the endocytosis FRET assay. PrP^C on the cell surface is first labeled with the donor FRET Eu-labeled antibody (t=0; 4 ºC). After removing excess antibody, cells are exposed to 37 ºC to initiate the uptake of Eu-labeled cell-surface PrP^C (t=1). During the course of internalisation Eu-labeled cell-surface PrP^C is endocytosed from the cell surface into the cell and residual Eu-labeled cell-surface PrP^C is measured by adding the acceptor FRET antibody at various time intervals (t=1-4). The endocytosis rate of PrP^C is calculated according to the uptake formula (see Experimental Procedures). (B) Time course of PrP^C endocytosis. A549 cells were first labeled with POM2-Eu at 4 ºC followed by the exposure to 37 ºC to initiate the internalization of PrP^C. At different time points (t=0 to 70 min) POM2-APC was added and the Net-FRET of the remaining cell surface POM2-Eu labeled PrP^C was measured. (C) Linear range of PrP^C internalization. Error bars represent the standard deviation (SD) of 6 replicate measurements. (D) Determination of the internalization rate. The PrP^C endocytosis index was calculated according to the formula in Experimental Procedures and reached a half life time of about 25 min. (E) Time course of cell surface PrP^C. A549 cells were labeled with POM2-Eu/POM2-APC at 4 ºC followed by the exposure to 37 ºC. The Net-FRET of cell surface PrP^C was measured at different time points.

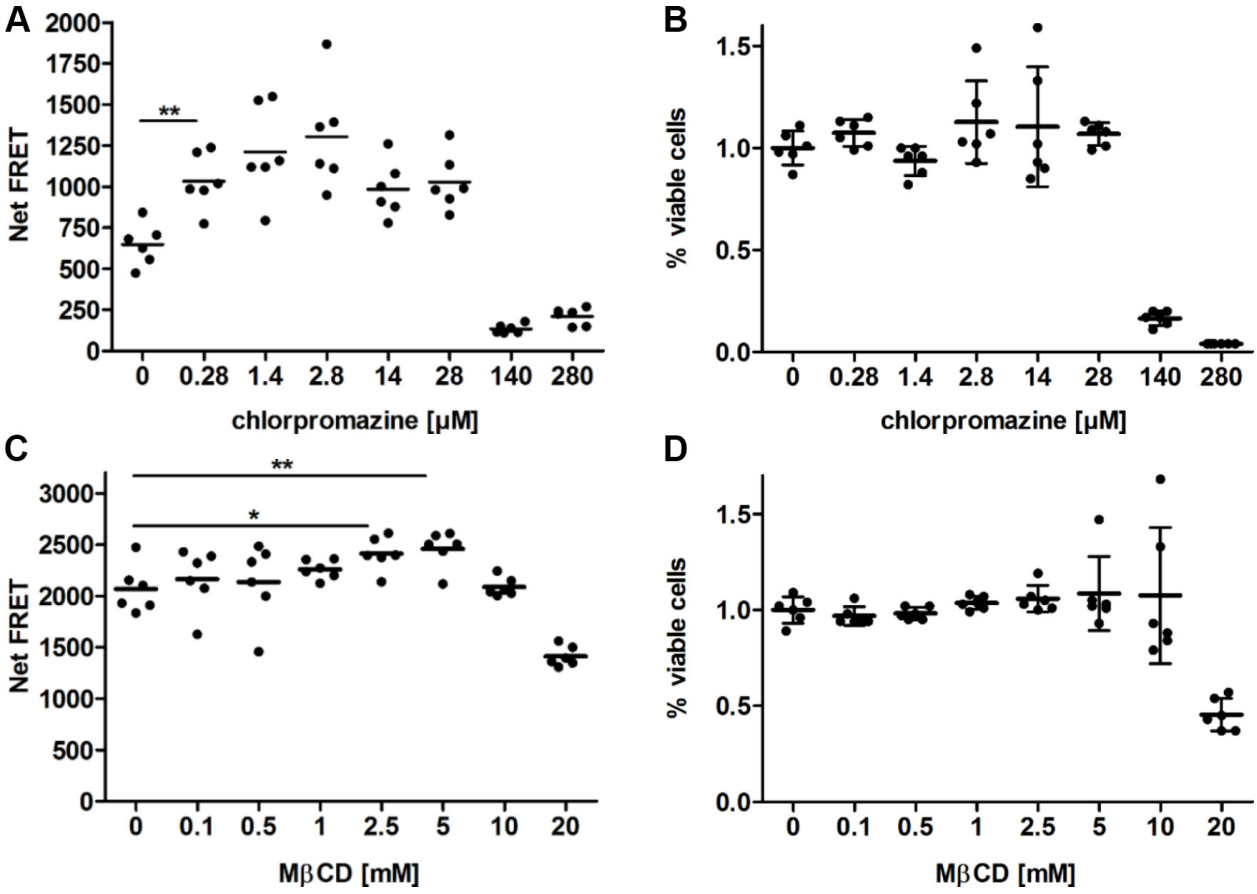

Figure 6: Effect of pharmaceutical compounds on PrP^C endocytosis. (A) A constant number of A549 cells was pre-labeled with POM2-Eu and treated with various concentrations of chlorpromazine. After 30 minutes of incubation, PrP^C endocytosis was assessed by the addition of POM2-APC. (B) Cell viability was measured by the alamarBlue assay. (C) Same as (A), but for MbetaCD. (D) Same as (B), but for MbetaCD. Error bars represent the standard deviation (± SD) of 6 replicate measurements. Student's t test: *: $p < 0.05$; **: $p < 0.01$; ***: $p < 0.001$; ****: $p < 0.0001$.

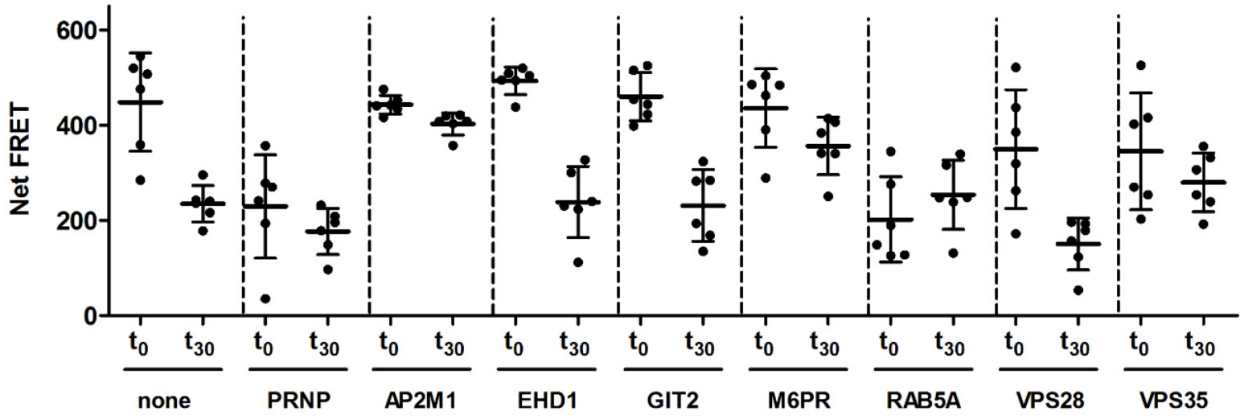

Figure 7: Manipulation of PrP^C endocytosis rate and cell surface expression by siRNA treatments. A549 cells were treated for three days with 50 nM siRNA. PrP^C internalization (t0-t30) and cell surface expression (t0) was measured by FRET using the antibody pair POM2-Eu/POM2-APC and the endocytosis rate (Table 4) was calculated according to the formula in Experimental Procedures. Untreated and PRNP siRNA treated cells were used as controls. Error bars represent the standard deviation (± SD) of 6 replicate measurements. Student's t test: *: $p < 0.05$; **: $p < 0.01$; ***: $p < 0.001$; ****: $p < 0.0001$.

Modifiers of prion protein biogenesis and recycling identified by a highly-parallel endocytosis kinetics assay

Boris A. Ballmer, Rita Moos, Prisca Liberali, Lucas Pelkmans, Simone Hornemann and Adriano Aguzzi

J. Biol. Chem. published online March 24, 2017

Access the most updated version of this article at doi: 10.1074/jbc.M116.773283